

Superfluid density and Berezinskii-Kosterlitz-Thouless transition of a spin-orbit coupled Fulde-Ferrell superfluid

Ye Cao^{1,2}, Xia-Ji Liu¹, Lianyi He³, Gui-Lu Long^{2,4,5}, and Hui Hu^{1*}

¹*Centre for Quantum and Optical Science, Swinburne University of Technology, Melbourne 3122, Australia*

²*State Key Laboratory of Low-dimensional Quantum Physics and Department of Physics, Tsinghua University, Beijing 100084, P. R. China*

³*Theoretical Division, Los Alamos National Laboratory, Los Alamos, NM87545, USA*

⁴*Collaborative Innovation Center of Quantum Matter, Beijing 100084, P. R. China and*

⁵*Tsinghua National Laboratory for Information Science and Technology, Beijing 100084, P. R. China*

(Dated: June 14, 2021)

We theoretically investigate the superfluid density and Berezinskii-Kosterlitz-Thouless (BKT) transition of a two-dimensional Rashba spin-orbit coupled atomic Fermi gas with both in-plane and out-of-plane Zeeman fields. It was recently predicted that, by tuning the two Zeeman fields, the system may exhibit different exotic Fulde-Ferrell (FF) superfluid phases, including the gapped FF, gapless FF, gapless topological FF and gapped topological FF states. Due to the FF pairing, we show that the superfluid density (tensor) of the system becomes anisotropic. When an in-plane Zeeman field is applied along the x -direction, the tensor component along the y -direction $n_{s,yy}$ is generally larger than $n_{s,xx}$ in most parameter space. At zero temperature, there is always a discontinuity jump in $n_{s,xx}$ as the system evolves from a gapped FF into a gapless FF state. With increasing temperature, such a jump is gradually washed out. The critical BKT temperature has been calculated as functions of the spin-orbit coupling strength, interatomic interaction strength, in-plane and out-of-plane Zeeman fields. We predict that the novel FF superfluid phases have a significant critical BKT temperature, typically at the order of $0.1T_F$, where T_F is the Fermi degenerate temperature. Therefore, their observation is within the reach of current experimental techniques in cold-atom laboratories.

PACS numbers: 05.30.Fk, 03.75.Hh, 03.75.Ss, 67.85.-d

I. INTRODUCTION

Over the past decade, the technique of manipulating ultracold atomic Fermi gases has been well developed and it offers a physical reality to pursue an exotic pairing mechanism, which is referred to as Fulde-Ferrell-Larkin-Ovchinnikov (FFLO) states [1, 2] and has attracted impressive attentions in different physical areas [3–7]. In spin-imbalanced Fermi gases, the standard Bardeen-Cooper-Schrieffer (BCS) pairing is not favorable against the FFLO pairing with a finite center-of-mass momentum. Although there is no unambiguous experimental conclusion for the FFLO superfluidity, strong evidence has been seen in a Fermi cloud of ${}^6\text{Li}$ atoms confined in quasi-one-dimensional harmonic traps near a crossover from a Bose-Einstein condensate (BEC) to a BCS superfluid [6, 8–12].

The FFLO pairing is also favored by spin-orbit coupling [13–17]. Motivated by the recent experimental realization of a synthetic spin-orbit coupling with equal weight combination of Rashba and Dresselhaus components [18–21], FF superfluidity - a specific form of the FFLO superfluidity - has been theoretically investigated in spin-orbit coupled atomic Fermi gases [22–30]. In the case of a Rashba spin-orbit coupling, topological superfluidity is argued to be achievable [31–38], although the

underlying pairing is of s -wave character. It turns out that the topological superfluidity and FF superfluidity are compatible. As a result, novel topological FF superfluids have also been proposed [39–45]. In particular, in a recent Letter, some of us have predicted that a *gapless* topological FF superfluid may appear in a two-dimensional (2D) spin-orbit coupled atomic Fermi gas with both in-plane and out-of-plane Zeeman fields [43]. The purpose of the present work is to provide more details about such an interesting superfluid phase and to discuss its thermodynamic stability by considering the superfluid density and superfluid transition temperature.

It is well known that at finite temperatures the superfluidity of 2D atomic Fermi gases is characterized by the vortex-antivortex (V-AV) binding. The relevant mechanism is the Berezinskii-Kosterlitz-Thouless (BKT) transition occurring at a characteristic temperature T_{BKT} [46, 47]. Below the critical BKT temperature, a V-AV binding state has a lower free energy and hence superfluidity emerges. The BKT transition was theoretically investigated long time ago in a 2D fermionic system without spin-orbit coupling [48–50]. Following the recent experimental advances, there have been several theoretical investigations about the superfluid density and critical BKT temperature in 2D spin-orbit coupled Fermi gases with BCS pairing [51–53]. In the case of a large out-of-plane Zeeman field, the temperature region for experimentally observing topological BCS superfluids and related Majorana fermions has been discussed [52, 53]. However, the BKT physics of a spin-orbit coupled FF

*Electronic address: hhu@swin.edu.au

superfluid - which can be either gapped or gapless, topologically trivial or non-trivial - has so far not been addressed.

In this work, we explore this interesting issue and study the superfluid density tensor and BKT transition of a 2D Rashba spin-orbit coupled Fermi gas in the presence of both in-plane and out-of-plane Zeeman fields. By calculating the superfluid density tensor, we obtain the superfluid phase stiffness as functions of the temperature, spin-orbit coupling strength, binding energy (that characterizes the interatomic interaction strength), in-plane and out-of-plane Zeeman fields. This allows us to determine the critical BKT temperature of the system in four different FF superfluid phases [43], with a given set of parameters.

Our main results may be summarized as follows: (i) At zero temperature with an applied in-plane Zeeman field in the x -direction, the component $n_{s,xx}$ of the superfluid density tensor always changes discontinuously when the system continuously evolves from a gapped FF into a gapless FF phase. The component $n_{s,yy}$ is larger than $n_{s,xx}$ except for a narrow parameter space where the FF momentum is sufficiently large. The two components of the superfluid density tensor decrease monotonically as the temperature increases. (ii) All the four FF superfluid phases have significant critical BKT temperature, except for the parameter region with very small spin-orbit coupling and/or binding energy, or with very large in-plane and/or out-of-plane Zeeman fields. The critical BKT temperature can be enhanced by increasing the binding energy. But it does not increase monotonically as the spin-orbit coupling strength increases.

The rest of the paper is organized as follows. In the next section, we briefly describe the mean-field theoretical framework, and clarify the BKT physics in two dimensions and the related Kosterlitz-Thouless-Nelson (KT-Nelson) criterion for phase transition. Then, we present the expressions for the superfluid density tensor and superfluid phase stiffness. The critical BKT temperature is determined by applying the KT-Nelson criterion. In Sec. III, we first present the finite-temperature phase diagram of the system and then discuss in detail the results on the superfluid density tensor and critical BKT temperature. Finally, Sec. IV is devoted to the conclusions and outlooks.

II. MODEL HAMILTONIAN AND MEAN-FIELD THEORY

We start by considering a 2D spin-orbit coupled two-component Fermi gas near a broad Feshbach resonance with the Rashba spin-orbit coupling $\lambda\hat{\sigma}\cdot\hat{\mathbf{k}}$, in-plane (h_x) and out-of-plane (h_z) Zeeman fields [54]. The system can be well described by the following single-channel Hamiltonian,

$$\mathcal{H} = \int d\mathbf{r} [\mathcal{H}_0 + \mathcal{H}_{int}], \quad (1)$$

where

$$\mathcal{H}_0 = \psi^\dagger(\mathbf{r}) \left(\hat{\xi}_{\mathbf{k}} + \lambda\hat{\sigma}\cdot\hat{\mathbf{k}} - h_z\hat{\sigma}_z - h_x\hat{\sigma}_x \right) \psi(\mathbf{r}) \quad (2)$$

is the single-particle Hamiltonian and

$$\mathcal{H}_{int} = U_0 \psi_\uparrow^\dagger(\mathbf{r}) \psi_\downarrow^\dagger(\mathbf{r}) \psi_\downarrow(\mathbf{r}) \psi_\uparrow(\mathbf{r}) \quad (3)$$

is the density of interaction Hamiltonian in which the bare interaction strength U_0 is to be regularized as

$$\frac{1}{U_0} = -\frac{1}{S} \sum_{\mathbf{k}} \frac{1}{\hbar^2 \mathbf{k}^2 / m + E_b}, \quad (4)$$

with S being the area of the system and E_b the two-particle binding energy that physically characterizes the interaction strength. In the single-particle Hamiltonian, λ is the Rashba spin-orbit coupling strength and we have used the following notations: (1) $\hat{\xi}_{\mathbf{k}} \equiv -\hbar^2 \nabla^2 / (2m) - \mu$ with the atomic mass m and chemical potential μ ; (2) $\hat{\mathbf{k}} = (\hat{k}_x, \hat{k}_y)$, where $\hat{k}_x = -i\partial_x$ and $\hat{k}_y = -i\partial_y$ are momentum operators; and (3) $\hat{\sigma} = (\hat{\sigma}_x, \hat{\sigma}_y)$, the Pauli matrices. We have also used $\psi(\mathbf{r}) = [\psi_\uparrow(\mathbf{r}), \psi_\downarrow(\mathbf{r})]^T$ ($\psi^\dagger(\mathbf{r}) = [\psi_\uparrow^\dagger(\mathbf{r}), \psi_\downarrow^\dagger(\mathbf{r})]$) to collectively denote the fermion field operator for creating (annihilating) an atom at \mathbf{r} with a specific spin $\sigma = \uparrow, \downarrow$.

A. Mean-field theory

We solve the model Hamiltonian Eq. (1) by using the functional path-integral approach [22, 53, 55, 56]. At the inverse finite temperature $\beta = 1/(k_B T)$, the partition function can be written as,

$$\mathcal{Z} = \int \mathcal{D}\psi(\mathbf{r}, \tau) \mathcal{D}\bar{\psi}(\mathbf{r}, \tau) \exp \{ -\mathcal{A}[\psi, \bar{\psi}] \}, \quad (5)$$

where

$$\mathcal{A}[\psi, \bar{\psi}] = \int_0^\beta d\tau \int d\mathbf{r} \bar{\psi} \partial_\tau \psi + \int_0^\beta d\tau \mathcal{H}(\psi, \bar{\psi}). \quad (6)$$

Here, the field operators ψ and ψ^\dagger in the model Hamiltonian \mathcal{H} have been replaced with the corresponding Grassmann variables $\psi(\mathbf{r}, \tau)$ and $\bar{\psi}(\mathbf{r}, \tau)$, respectively. Following the standard procedure [22], the interaction term in the Hamiltonian is decoupled using the Hubbard-Stratonovich transformation. Introducing the auxiliary complex pairing field $\phi(\mathbf{r}, \tau) = -U_0 \psi_\downarrow(\mathbf{r}, \tau) \psi_\uparrow(\mathbf{r}, \tau)$, and integrating out the Grassmann fields, the partition function becomes

$$\mathcal{Z} = \int \mathcal{D}\phi(\mathbf{r}, \tau) \mathcal{D}\bar{\phi}(\mathbf{r}, \tau) \exp \{ -\mathcal{A}_{eff}[\phi, \bar{\phi}] \}, \quad (7)$$

where in the saddle-point approximation (i.e., mean-field treatment by replacing $\phi(\mathbf{r}, \tau)$ with a static pairing field $\Delta(\mathbf{r})$), the effective action \mathcal{A}_{eff} takes the form,

$$\mathcal{A}_{mf} = \beta \sum_{\mathbf{k}} \hat{\xi}_{\mathbf{k}} - \int_0^\beta d\tau \int d\mathbf{r} \frac{|\Delta|^2}{U_0} - \frac{1}{2} \text{Tr} \ln [-G^{-1}]. \quad (8)$$

In the above expression, $G^{-1}(\mathbf{r}, \tau) = -\partial_\tau - \mathcal{H}_{BdG}$ is the inverse single-particle Green function in the Nambu-Gorkov representation, with a mean-field Bogoliubov Hamiltonian,

$$\mathcal{H}_{BdG} = \begin{bmatrix} H_0(\hat{\mathbf{k}}) & -i\Delta(\mathbf{r})\hat{\sigma}_y \\ i\Delta(\mathbf{r})\hat{\sigma}_y & -H_0^*(-\hat{\mathbf{k}}) \end{bmatrix}, \quad (9)$$

where $H_0 \equiv \hat{\xi}_{\mathbf{k}} + \lambda \hat{\sigma} \cdot \hat{\mathbf{k}} - h_z \hat{\sigma}_z - h_x \hat{\sigma}_x$. In the presence of the in-plane Zeeman field h_x , it is known that the pairing field takes the FF form $\Delta(\mathbf{r}) = \Delta e^{iQx}$, with a finite center-of-mass momentum of the pairs $\mathbf{Q} = Q\mathbf{e}_x$ [24–28]. This helical phase was earlier studied in the context of noncentrosymmetric superconductors [15, 16]. The resulting mean-field thermodynamic potential $\Omega_{mf} = k_B T \mathcal{A}_{mf}$ reads,

$$\Omega_{mf} = \sum_{\mathbf{k}} \hat{\xi}_{\mathbf{k}} - \mathcal{S} \frac{\Delta^2}{U_0} - \frac{k_B T}{2} \sum_{\mathbf{k}, i\omega_m} \ln \det [-G^{-1}(\mathbf{k}, i\omega_m)], \quad (10)$$

where $G^{-1}(\mathbf{k}, i\omega_m)$ is the inverse Green function in momentum space and $\omega_m = \pi(2m+1)/\beta$ with integer m is the fermionic Matsubara frequency. Making use of the inherent particle-hole symmetry of the BdG Hamiltonian, we find that,

$$\det [-G^{-1}(\mathbf{k}, i\omega_m)] = \prod_{\eta=1,2} \left[(i\omega_\eta)^2 - \left(E_{\mathbf{k}\eta}^{\nu=\pm} \right)^2 \right], \quad (11)$$

where $E_{\mathbf{k}\eta}^\nu$ is the quasi-particle energy, obtained by diagonalizing \mathcal{H}_{BdG} with the FF pairing field $\Delta(\mathbf{r}) = \Delta e^{iQx}$ [26, 27]. The superscript $\nu \in (+, -)$ represents the particle (+) or hole (–) branch and the subscript $\eta \in (1, 2)$ denotes the upper (1) or lower (2) branch split by the spin-orbit coupling [26, 55, 56]. By summing over the Matsubara frequency, the mean-field thermodynamic potential takes the form,

$$\begin{aligned} \Omega_{mf} &= \frac{1}{2} \sum_{\mathbf{k}} (\xi_{\mathbf{k}+\mathbf{Q}/2} + \xi_{\mathbf{k}-\mathbf{Q}/2}) - \frac{1}{2} \sum_{\mathbf{k}\eta} |E_{\mathbf{k}\eta}^+| \\ &\quad - k_B T \sum_{\mathbf{k}\eta} \ln \left(1 + e^{-|E_{\mathbf{k}\eta}^+|/k_B T} \right) - \mathcal{S} \frac{\Delta^2}{U_0}. \end{aligned} \quad (12)$$

Here the term $\sum_{\mathbf{k}} \hat{\xi}_{\mathbf{k}}$ is replaced by $(1/2) \sum_{\mathbf{k}} (\xi_{\mathbf{k}+\mathbf{Q}/2} + \xi_{\mathbf{k}-\mathbf{Q}/2})$, in order to cancel the leading divergence of the term $(1/2) \sum_{\mathbf{k}\eta} |E_{\mathbf{k}\eta}^+|$.

For a given set of parameters, for example, the temperature T , binding energy E_b etc., different superfluid phases can be determined using the self-consistent stationary conditions:

$$\frac{\partial \Omega_{mf}}{\partial \Delta} = 0, \quad (13)$$

$$\frac{\partial \Omega_{mf}}{\partial Q} = 0, \quad (14)$$

as well as the conservation of total atom number,

$$n = -\frac{1}{\mathcal{S}} \frac{\partial \Omega_{mf}}{\partial \mu}, \quad (15)$$

where $n = N/\mathcal{S}$ is the number density. At a given temperature, the ground state has the lowest free energy $F = \Omega_{mf} + \mu N$.

B. Superfluid density tensor

An important quantity to characterize the anisotropic superfluid properties of a 2D spin-orbit coupled Fermi gas is the superfluid density tensor. In the case of BCS pairing, the superfluid density tensor may be analytically derived within mean-field framework [51, 52, 57], yet the formalism has not been obtained for a FF superfluid. According to the definition of the superfluid density, we calculate it by applying a phase twist to the order parameter, $\Delta_{twist}(\mathbf{v}_s) = \Delta(\mathbf{r}) e^{i\mathbf{q} \cdot \mathbf{r}}$, which boosts the system with a uniform superfluid flow at a velocity $\mathbf{v}_s = \hbar \mathbf{q}/2m$ [57–59]. Here $\Delta(\mathbf{r})$ is the equilibrium FF order parameter. Physically, only the superfluid component moves under the influence of the superfluid flow. Thus, as the result of this boost, the thermodynamic potential assumes the following form in the limit of small velocity,

$$\Omega(\mathbf{v}_s) \simeq \Omega(\mathbf{v}_s = 0) + \frac{1}{2} m \mathcal{S} \sum_{ij} n_{s,ij} v_{si} v_{sj}, \quad (16)$$

where $n_{s,ij}$ ($i, j = x, y$) is the superfluid density tensor. Therefore, we immediately obtain [57–59],

$$n_{s,ij} = \frac{1}{\mathcal{S}} \frac{4m}{\hbar^2} \left[\frac{\partial^2 \Omega(\mathbf{v}_s)}{\partial q_i \partial q_j} \right]_{\mathbf{q}=0}, \quad (17)$$

where $\Omega(\mathbf{v}_s)$ should be calculated with $\Delta_{twist}(\mathbf{v}_s)$ in the presence of the phase twist. The above relation for the superfluid density tensor is rigorous. In this work, consistent with the mean-field treatment for thermodynamics, in Eq. (17) we shall approximate the thermodynamic potential $\Omega(\mathbf{v}_s)$ by its mean-field value $\Omega_{mf}(\mathbf{v}_s)$.

C. The KT-Nelson criterion for T_{BKT}

The BKT transition in 2D is peculiar, associated with the spontaneous vortex formation. A unique feature of

such a transition is a universal jump in the superfluid density (tensor), characterized by the KT-Nelson criterion for the critical BKT temperature [60]. It may be explained by using the following simple physical picture for the spontaneous creation of a single vortex at finite temperature T .

In the absence of spin-orbit coupling and Zeeman fields, let us consider an *isotropic* Fermi superfluid in a circular disk geometry, with a radius of $R \rightarrow \infty$. The kinetic energy cost for creating a single vortex at the origin $\mathbf{r} = \mathbf{0}$ is simply given by,

$$E_V \simeq \frac{1}{2} m n_s \int_{\xi}^R d^2 \mathbf{r} \left(\frac{\hbar}{2mr} \right)^2 = \frac{\hbar^2 \pi}{4m} n_s \ln \left(\frac{R}{\xi} \right), \quad (18)$$

where ξ is the size of the vortex core. The associated entropy can be calculated by the number of distinct positions at which the vortex can be placed,

$$S_V \simeq k_B \ln \left(\frac{\pi R^2}{\pi \xi^2} \right) = 2k_B \ln \left(\frac{R}{\xi} \right). \quad (19)$$

From these two expressions, we see that the free energy associated with the formation of a single vortex is,

$$F_V = E_V - T S_V \simeq 2 \left(\frac{\pi \hbar^2}{2} \frac{n_s}{4m} - k_B T \right) \ln \left(\frac{R}{\xi} \right). \quad (20)$$

It is clear that the free energy changes its sign at a characteristic temperature T_{BKT} determined by

$$k_B T_{BKT} = \frac{\pi}{2} \mathcal{J}, \quad (21)$$

where $\mathcal{J} = \hbar^2 n_s / (4m)$ is the superfluid phase stiffness. This is the well-known KT-Nelson criterion [60]. As $\ln(R/\xi)$ diverges in the thermodynamic limit $R \rightarrow \infty$, the temperature T_{BKT} separates two qualitatively different regimes. At $T > T_{BKT}$, the free energy is very large and negative, suggesting the spontaneous creation of a free vortex with either positive or negative circulation. While at $T < T_{BKT}$, vortices with opposite circulation will bind together and generate coherence. The spontaneous creation of free vortex suggests that the loss of the phase coherence of the system occurs suddenly. It leads to a universal jump in the superfluid phase stiffness or superfluid density, as can be seen clearly from the KT-Nelson criterion, Eq. (21).

In the case of an *anisotropic* superfluid, we need to define a superfluid density tensor

$$\mathcal{N}_s = \begin{bmatrix} n_{s,xx} & n_{s,xy} \\ n_{s,yx} & n_{s,yy} \end{bmatrix}. \quad (22)$$

The associated superfluid phase stiffness takes the form,

$$\mathcal{J} = \frac{\hbar^2}{4m} (\det \mathcal{N}_s)^{1/2} = \frac{\hbar^2}{4m} \sqrt{n_{s,xx} n_{s,yy}}, \quad (23)$$

where in the last equation, we use the fact that $n_{s,xy} = n_{s,yx} = 0$, which holds for the system considered in this work.

It is worth noting that although Eq. (21) is obtained by drawing a simple physical picture, it would be a rigorous criterion for the BKT transition. Indeed, the KT-Nelson criterion was first obtained by using a renormalization group analysis [60]. For a microscopic derivation, we may consider the contribution of the pair fluctuations around the saddle-point solution $\delta\phi(\mathbf{q}, i\nu_n)$ to the action $\delta\mathcal{A}$, which, at the *Gaussian* (quadratic) level, is given by [51, 53, 61, 62],

$$\delta\mathcal{A} = \frac{1}{2} \sum_{\mathcal{Q}=\mathbf{q}, i\nu_n} [\delta\phi^\dagger(\mathcal{Q}), \delta\phi(-\mathcal{Q})] \mathbf{M} \begin{bmatrix} \delta\phi(\mathcal{Q}) \\ \delta\phi^\dagger(-\mathcal{Q}) \end{bmatrix}, \quad (24)$$

where the 2×2 matrix

$$\mathbf{M} \equiv \begin{bmatrix} M_{11}(\mathcal{Q}), & M_{12}(\mathcal{Q}) \\ M_{21}(\mathcal{Q}), & M_{22}(\mathcal{Q}) \end{bmatrix} \quad (25)$$

is the inverse two-particle (pair) propagator and its elements can be evaluated with the mean-field fermionic Green function $G(\mathbf{k}, i\omega_m)$. In the case of BCS pairing without the in-plane Zeeman field, the expression of the inverse pair propagator \mathbf{M} can be analytically obtained [53, 61]. In particular, in the limit of long wavelength, the matrix elements of \mathbf{M} can be expanded as functions of small \mathbf{k} and ω . By separating the phase fluctuation and amplitude (density) fluctuation, the low-energy physics of the system can be found to be governed by the well-known classical spin XY model [53, 61], which is the prototype of the BKT physics. In this way, one microscopically derives the superfluid phase stiffness \mathcal{J} and the KT-Nelson relation. The resulting expression for the superfluid phase stiffness *coincides* with the mean-field phase stiffness obtained, for example, by using the mean-field thermodynamic potential in Eq. (17). In our FF case, the expression of the superfluid phase stiffness could be derived in a similar manner. However, in this case, the analytical expression of the inverse pair propagator \mathbf{M} is more difficult to obtain, although we can numerically sum over the bosonic Matsubara frequency $i\nu_n$. Therefore, to calculate the superfluid phase stiffness, we prefer to directly use Eq. (17) with a mean-field thermodynamic potential.

D. Pair fluctuations beyond mean-field

To close this section, we briefly discuss how to improve the mean-field theory. An immediate idea is to work out the Gaussian correction to the action, $\delta\mathcal{A}$, and then use the improved thermodynamic potential around the saddle point $\Delta(\mathbf{r}) = \Delta e^{i\mathcal{Q}x}$ [58, 59, 63],

$$\Omega_{GPF} = \Omega_{mf} + k_B T \sum_{\mathcal{Q}=\mathbf{q}, i\nu_n} \ln \mathbf{M}(\mathcal{Q}), \quad (26)$$

to calculate the equation of state through the standard thermodynamic relations and the superfluid density tensor via Eq. (17). In this way, the thermodynamics and

the superfluid density tensor of the system can be consistently determined at the same level of approximation. Alternatively, we may also consider using Ω_{GPF} to determine the chemical potential μ and then calculate the superfluid density tensor using the mean-field expression. However, as the trade-off of this cheap treatment, we may have an inconsistency. The resulting critical BKT temperature could be less reliable. For a detailed discussion, we refer to the recent work by Tempere and Klimin [64].

III. RESULTS AND DISCUSSIONS

Using the above-mentioned mean-field theoretical framework, we have systematically explored the low-temperature phase diagram and the thermodynamic stability of different exotic Fulde-Ferrell superfluid phases. In our numerical calculations, we take the Fermi wavevector $k_F = \sqrt{2\pi n}$ and the Fermi energy $E_F = \hbar^2 k_F^2 / (2m)$ as the units for wavevector and energy, respectively. For a typical set of parameters (i.e., default parameters), we use the interaction parameter $E_b = 0.2E_F$, spin-orbit coupling strength $\lambda = E_F/k_F$, in-plane Zeeman field $h_x = 0.4E_F$, out-of-plane Zeeman field $h_z = 0.1E_F$ and temperature $T = 0.05T_F$.

A. Low-temperature phase diagrams

In the recent Letter [43], we have discussed the phase diagram and the appearance of an interesting gapless topological Fulde-Ferrell superfluid at a weak interaction strength parameterized by $E_b = 0.2E_F$. Experimentally, it is most likely that the measurement will be carried out at a stronger interaction strength, where the superfluid transition temperature is anticipated to be higher. In order to optimize the experimental condition for observing the gapless topological superfluid, here we present a systematic study with varying binding energy, from the weakly interacting BCS side to the strongly interacting BEC-BCS crossover regime.

In Fig. 1, we report two phase diagrams at the typical low temperature $T = 0.05T_F$ on the plane of E_b - h_x (a) or E_b - h_z (b). The superfluid phase stiffness $\pi\mathcal{J}/2$ in different phases is color illustrated and its detailed behavior will be discussed in the next subsection. The superfluid phases are determined using the KT-Nelson criterion $\pi\mathcal{J}(T = 0.05T_F)/2 > k_B T = 0.05E_F$. Obviously, there is a pseudogap regime (shown in grey), in which the pairing order parameter is finite but the superfluid phase stiffness is not large enough to drive the BKT transition. A better understanding of the pseudogap phase requires a careful treatment of strong phase fluctuations. It is out of the scope of the present paper.

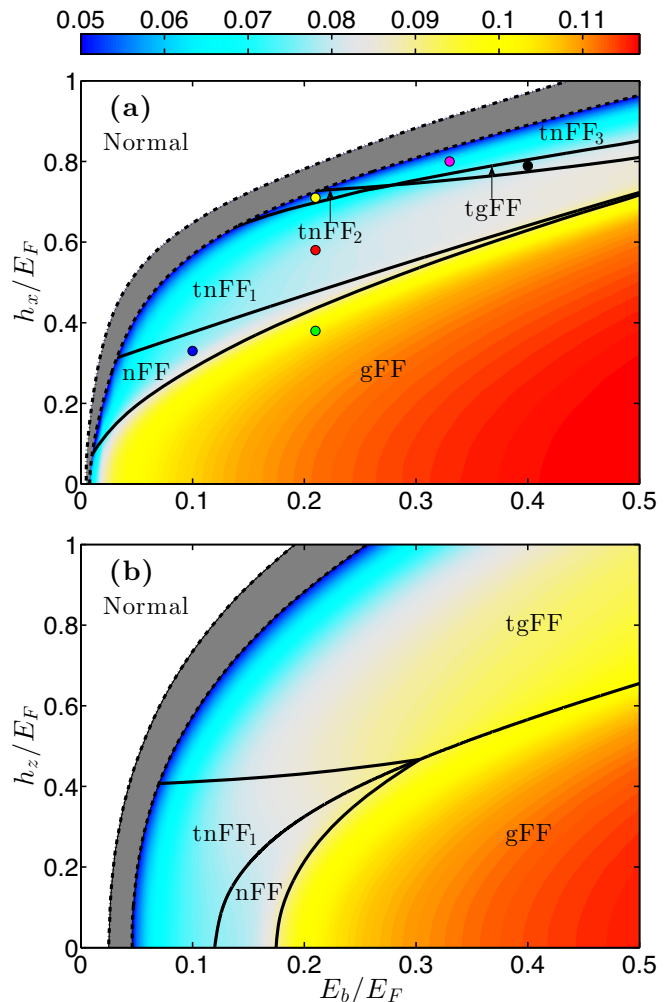


Figure 1: (color online) Phase diagrams of a 2D spin-orbit coupled atomic Fermi gas at a broad Feshbach resonance and at a typical low temperature $0.05T_F$ with (a) $h_x = 0.1E_F$ or (b) $h_z = 0.4E_F$. The strength of spin-orbit coupling is $\lambda = E_F/k_F$. There are four superfluid phases: gFF, nFF, tnFF and tgFF (whose phase stiffness $\pi\mathcal{J}/2$ - in units of E_F - is illustrated in color), as well as a pseudogap phase (grey area). We treat the system as a normal gas (shown in white) when the pairing gap $\Delta < 10^{-3}$. In the gapless topological phase, the notations tnFF₁, tnFF₂ and tnFF₃ distinguish different zero-energy contours in energy spectrum. For details, see the contour plots in Fig. 2.

1. gapless topological transition

It is known from previous studies [41–43] that the combined effect of spin-orbit coupling, in-plane and out-of-plane Zeeman fields may induce several exotic superfluid phases: gapped FF (gFF), gapless FF (nFF), gapless topological FF (tnFF) and gapped topological FF (tgFF), classified by considering whether the system has a bulk-gapped and/or topologically non-trivial energy spectrum. In the literature, the topological superfluidity was firstly studied with an out-of-plane Zeeman field

only [22, 31]. In that case, topological phase transition can be driven by increasing the out-of-plane Zeeman field h_z above a threshold

$$h_{z,c} = \sqrt{\Delta^2 + \mu^2}, \quad (27)$$

at which the dispersions of the particle- and hole-branches touch each other at the single point $\mathbf{k} = 0$, meanwhile the bulk excitation gap closes. Afterwards, the topology of the Fermi surface dramatically changes and the excitation gap re-opens [22, 65, 66]. It is straightforward to understand the single-point closure of the excitation gap, since the Fermi surface is always rotationally symmetric. This also implies that the resulting topological superfluid must be gapped in the bulk. However, such a scenario may be greatly altered by the presence of a non-zero in-plane Zeeman field, which favors the FF pairing with a finite center-of-mass momentum and consequently breaks the rotational symmetry of the Fermi surface.

In the case of a small in-plane Zeeman field, the rotational symmetry breaking of the energy spectrum is not significant. Although the system becomes a FF superfluid, its bulk excitation gap still closes at the single point $\mathbf{k} = 0$, accompanied by the change of the topology of the Fermi surface. An example is the transition from gFF to tgFF shown in Fig. 1(b) at large binding energy $E_b > 0.3E_F$, where the in-plane Zeeman field is effectively weak. As a result, the picture of the out-of-plane field induced topological phase transition remains unchanged [40–42].

When the in-plane Zeeman field keeps increasing over a threshold $h_{x,c1}$, however, the closure of the excitation gap and the change of the topology of the Fermi surface may not occur at the same time. A gapless superfluid phase - referred to as nFF - may emerge in the first place at $\mathbf{k} \neq 0$. The nodal points with $E_{\eta=2}^{\nu}(k_x, k_y) = 0$ form two disjoint loops (see, for example, the transition from gFF to nFF in Fig. 1(a)). The topology of the Fermi surface only changes when the in-plane Zeeman field further increases up to another critical value $h_{x,c2}$, at which the two nodal loops connect at $\mathbf{k} = 0$. We refer to the previous work Ref. [43] for a detailed characterization of the gapless topological transition.

2. Binding energy dependence of the phase diagram

It can now be understood that both the in-plane and out-of-plane fields can drive the topological phase transition, but the underlying property of the resulting topological phase, in terms of the gapless or gapped bulk spectrum, depends critically on the relative strength of the two fields. The gapless topological FF superfluid (tnFF) intentionally emerges in the parameter regime where h_x is larger enough relative to h_z .

This is particularly clear from Fig. 1(a), where we have fixed the strength of the out-of-plane Zeeman field to $h_z = 0.1E_F$. The tnFF phase accounts for most of the

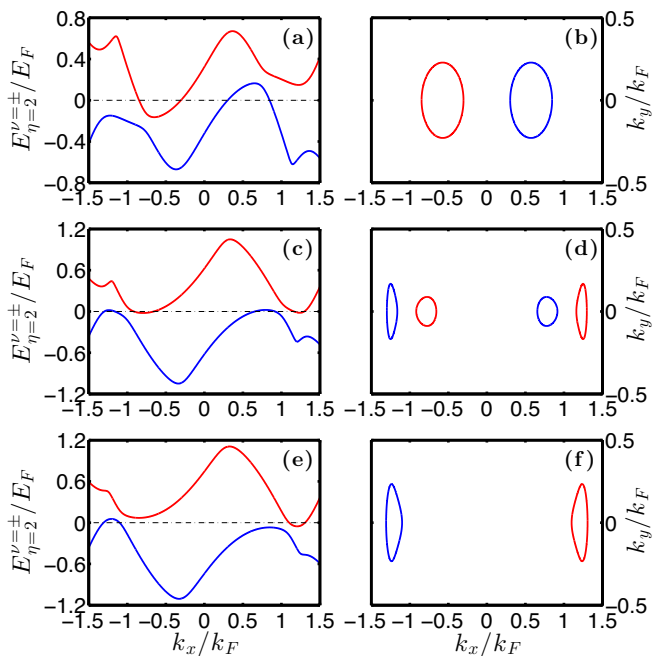


Figure 2: (color online) Dispersion relation of the lower branch $E_{\eta=2}^{\nu}(k_x, k_y = 0)$ (left panel, red curves for particle excitations $\nu = +$ and blue curves for hole excitations $\nu = -$) and the corresponding contour of zero-energy nodes (right panel). (a) and (b) correspond to the red point in Fig. 1 for the tnFF₁ phase, (c) and (d) the yellow point for the tnFF₂ phase and, (e) and (f) the magenta point for the tnFF₃ phase.

space for topological phases. It is remarkable that the window of the tnFF superfluid remains very significant when the binding energy increases up to $0.5E_F$, suggesting the use of a large interaction strength near Feshbach resonances, for the purpose of having a larger BKT transition temperature to observe the exotic tnFF phase. On the contrary, Fig. 1(b) - where we have fixed the in-plane Zeeman field to $h_x = 0.4E_F$ - clearly reveals that the gapped topological FF superfluid (tgFF) occupies most of the space for topological phases, when the out-of-plane Zeeman field is larger than the in-plane Zeeman field. In this case, the tnFF phase is restricted to the parameter space with a small out-of-plane Zeeman field and a weak interaction strength, as one may anticipate.

3. Different gapless topological superfluid phases

It is interesting that the gapless topological FF superfluid may be further classified into different categories (tnFF₁, tnFF₂ and tnFF₃), according to the number and position of its disjoint loops of nodal points, as shown in the right panel of Fig. 2. The tnFF₁ superfluid is most common and has two nodal loops, one for the particle branch (red loop) and another for the hole branch (blue loop). The tnFF₃ superfluid also has two nodal loops. However, the loops for the particle and hole branches ex-

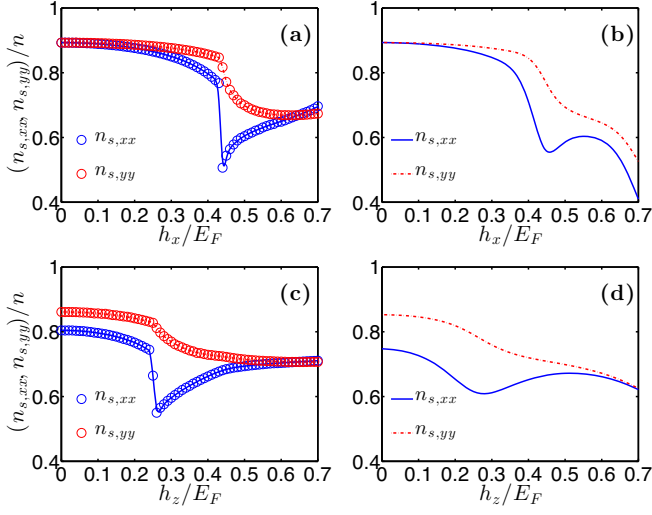


Figure 3: (color online) Diagonal elements of the superfluid density tensor as a function of h_x and h_z at zero temperature (left panel) and at a finite temperature $T = 0.05T_F$ (right panel). The superfluid density is measured in units of the total density $n = k_F^2/(2\pi)$. In (a) and (b), the out-of-plane Zeeman field strength $h_z = 0.1E_F$. In (c) and (d), the in-plane Zeeman field strength $h_x = 0.4E_F$. Other parameters are $E_b = 0.2E_F$ and $\lambda = E_F/k_F$.

change their position. It occurs only at large in-plane Zeeman field and binding energy. The tnFF₂ seems to connect the tnFF₁ and tnFF₃ phases. It has four disjoint nodal loops and exists only in a very narrow parameter space (see, for example, Fig. 1(a)). We note that the two gapless topological phases, tnFF₁ and tnFF₃, may also be intervened by a *gapped* topological phase, in which there is no nodal loop at all.

B. Superfluid density

Having determined the low-temperature phase diagram, we are in position to understand the superfluid density and the critical BKT temperature of different superfluid phases, which have been only briefly mentioned in our previous Letter [43]. In the presence of spin-orbit coupling, it is known that the superfluid density is a tensor [51, 53]. We then have to consider both diagonal elements of the superfluid density tensor, $n_{s,xx}$ and $n_{s,yy}$.

In Fig. 3, we present the Zeeman field dependence of $n_{s,xx}$ and $n_{s,yy}$ at zero temperature (left panel, a and c) and at a finite temperature $T = 0.05T_F$ (right panel, b and d). In general, as a consequence of the in-plane Zeeman field applied along the x -axis, $n_{s,xx}$ is smaller than $n_{s,yy}$, except at extremely low temperature and sufficiently large Zeeman fields.

At zero temperature, $n_{s,xx}$ initially decreases with increasing Zeeman fields and exhibits a sudden drop when the system evolves from the gFF phase into the nFF phase at the threshold $h_{x,c1}$ (or $h_{z,c1}$). At $h_x > h_{x,c1}$

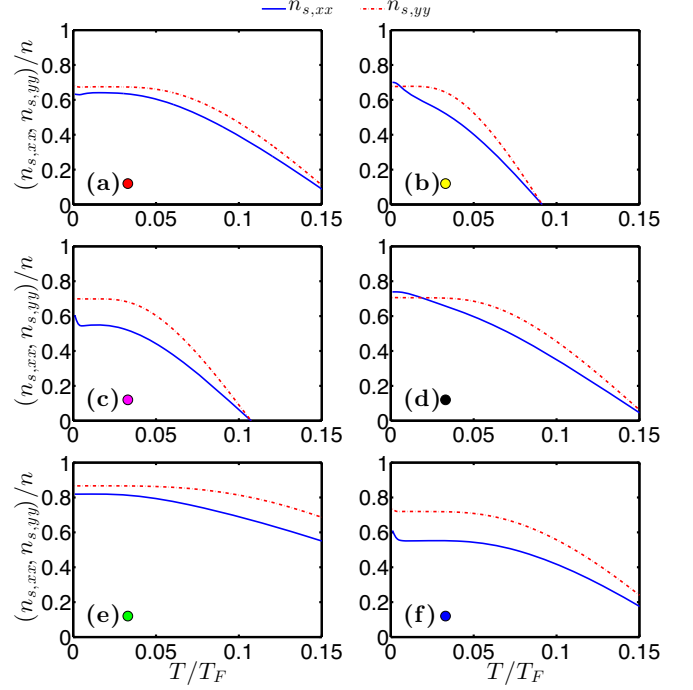


Figure 4: (color online) Temperature dependence of the diagonal elements of the superfluid density tensor, at the six points shown in Fig. 1(a): (a) $E_b = 0.21E_F$ and $h_x = 0.58E_F$, the tnFF₁ phase; (b) $E_b = 0.21E_F$ and $h_x = 0.71E_F$, the tnFF₂ phase; (c) $E_b = 0.33E_F$ and $h_x = 0.8E_F$, the tnFF₃ phase; (d) $E_b = 0.4E_F$ and $h_x = 0.789E_F$, the tgFF phase; (e) $E_b = 0.21E_F$ and $h_x = 0.2E_F$, the gFF phase; and (f) $E_b = 0.1E_F$ and $h_x = 0.33E_F$, the nFF phase. The superfluid density is measured in units of the total density $n = k_F^2/(2\pi)$. Other parameters are $h_z = 0.1E_F$ and $\lambda = E_F/k_F$.

(or $h_z > h_{z,c1}$) it then rises up gradually and is always enhanced by the Zeeman field. Apart from the discontinuous jump, similar Zeeman-field dependence of the superfluid density has been reported for a gapped BCS topological superfluid across the topological phase transition [53]. Compared with the non-monotonic field dependence of $n_{s,xx}$, we always find that $n_{s,yy}$ decreases continuously with increasing the Zeeman field. Instead of the sudden drop, a kink is observed at the transition from the gFF phase to the nFF phase.

The behavior of the superfluid density is profoundly affected by a nonzero temperature. Already at $T = 0.05T_F$, the discontinuous drop in $n_{s,xx}$ is smoothed out, leaving a broad minimum with a width $\Delta h_{x,z} \sim 2k_B T = 0.1E_F$. Moreover, at the large Zeeman field $h_{x,z} \sim 0.6E_F$, $n_{s,xx}$ starts to decrease with increasing the Zeeman field. At even higher temperature (not shown in the figure), the local minimum in $n_{s,xx}$ may disappear.

In Fig. 4, we report the temperature dependence of the superfluid density at six typical sets of parameters, which correspond to different superfluid phases at $T = 0.05T_F$, as shown in Fig. 1(a). $n_{s,xx}$ and $n_{s,yy}$ decrease as temperature increases, in agreement with the common idea

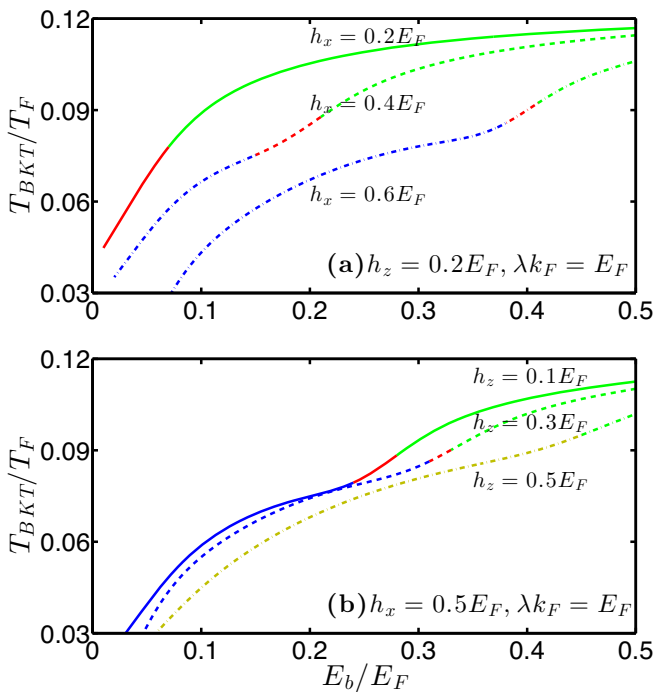


Figure 5: (color online) The critical BKT transition temperature as a function of the binding energy E_b at different in-plane Zeeman fields (a) or out-of-plane Zeeman fields (b). Here and in the next two figures, the color green, red, blue and yellow in the curves denote the superfluid phase gFF, nFF, tnFF and tgFF, respectively.

that the superfluid component should be gradually destroyed by thermal excitations. It is remarkable that for the gapless topological tnFF₁ phase (see Fig. 4(a)), the superfluid density does not decrease rapidly with increasing temperature, implying a sizable critical BKT transition temperature for its experimental observation, as we shall discuss in greater detail in the next subsection. In contrast, the superfluid density of other two gapless topological phases (tnFF₂ and tnFF₃ in Figs. 4(b) and 4(c), respectively) is more sensitive to temperature and vanishes at $T \sim 0.1T_F$, probably due to their large Zeeman fields.

C. Critical BKT temperature and finite-temperature phase diagrams

We now turn to consider the critical BKT temperature, which is determined by the KT-Nelson criterion,

$$k_B T_{BKT} = \frac{\pi \hbar^2}{8m} [n_{s,xx}(T_{BKT}) n_{s,yy}(T_{BKT})]^{1/2}. \quad (28)$$

In the above equation, we have explicitly written down the temperature dependence of the superfluid density, in order to emphasize the fact that the critical BKT temperature should be solved self-consistently. In Figs. 5, 6 and 7, we show the results as a function of the binding

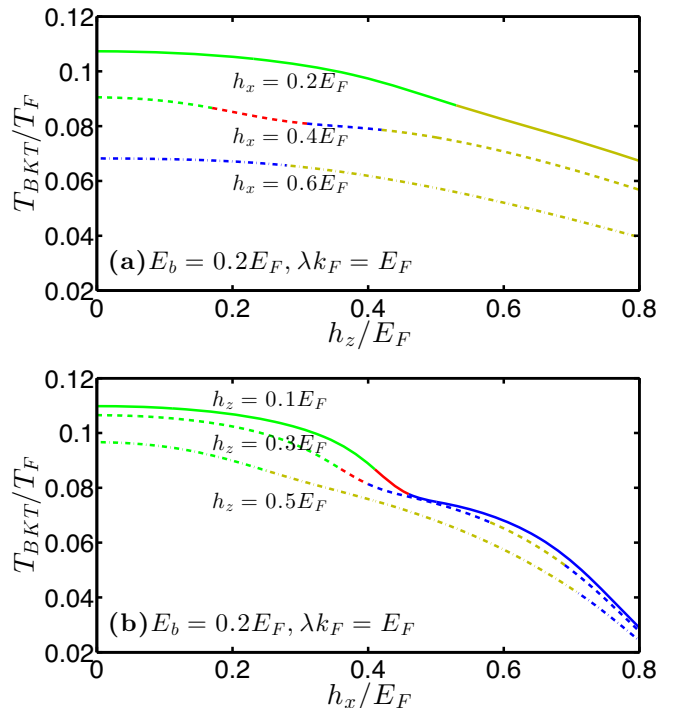


Figure 6: (color online) The critical BKT transition temperature as a function of the out-of-plane Zeeman field h_z (a) or the in-plane Zeeman field h_x (b).

energy, Zeeman fields and spin-orbit coupling strength, respectively. These results should be regarded as finite-temperature phase diagrams, as they show clearly which kind of superfluid phases is preferable when temperature decreases. In the curves, we use different colors to distinguish different *emerging* superfluid phases: green for the gFF phase, red for the nFF phase, blue for the tnFF phase and finally yellow for the tgFF phase. It is clear that all the four FF superfluid phases have significant critical BKT temperature except for the parameter regime with very small binding energy E_b and/or spin-orbit coupling strength λ , or with very large in-plane Zeeman field h_x and/or out-of-plane Zeeman field h_z .

As illustrated in Fig. 5, the critical BKT temperature T_{BKT} always increases monotonically with increasing the binding energy E_b , as the pairing and superfluidity are enhanced at strong interatomic interactions. The binding energy is the dominant factor in forming Cooper pairs. With a small binding energy, the system is mainly of fermionic character. On the contrary, with a sufficiently large binding energy, the system tends to act as a gas of bosons. Therefore, with increasing the binding energy up to some points, the system would lose its fermionic character near the BEC-BCS crossover (i.e., $E_b \sim 0.5E_F$) and hence should become topologically trivial. Indeed, at large binding energy we observe that the system always approaches the topologically trivial gFF phase. The topological phase, either gapless (tnFF in blue) or gapped (tgFF in yellow), is favored at small binding energy,

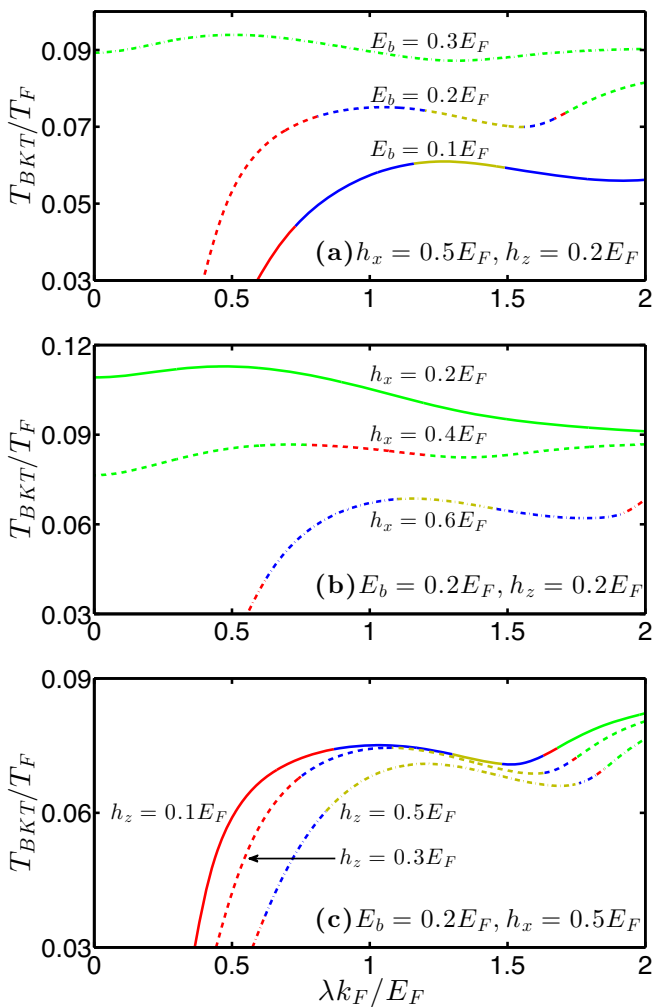


Figure 7: (color online) The critical BKT transition temperature as a function of the spin-orbit coupling strength λ at different binding energies (a), in-plane Zeeman fields (b) and out-of-plane Zeeman fields (c).

where the critical BKT temperature is lower. Nevertheless, we find that by suitably tuning the parameters, it is possible to have a gapless topological tnFF phase with a sizable critical BKT temperature $T_{BKT} \sim 0.09T_F$ for the binding energy up to $E_b \simeq 0.4E_F$ (see, for example, the dot-dashed line at the bottom of Fig. 5(a)). This temperature is clearly within the reach in current cold-atom experiments [67].

On the other hand, the critical BKT temperature decreases monotonically with increasing the Zeeman field, either in-plane or out-of-plane, as shown in Fig. 6. It is readily seen that with decreasing temperature the system would first turn into either the tnFF or tgFF phase at sufficiently large in-plane Zeeman field h_x or out-of-plane field h_z , respectively. While at low Zeeman fields, the topologically trivial gFF phase is preferable. This agrees the observation we made in discussing the low-temperature phase diagrams in Fig. 1.

It is worth noting that, one may use the binding en-

ergy dependence or the Zeeman field dependence of the critical BKT temperature to identify different emerging superfluid phases. This is particularly clear for the gapless tnFF and nFF phases, as the curvature of the T_{BKT} curve for those phases behaves quite differently. For the tnFF phase, the curve is concave; while for the nFF phase, it is convex. This change in curvature (i.e., from concave to convex) seems to be related to the local minimum in the superfluid density component $n_{s,xx}$ that we have reported earlier in Fig. 3.

We now discuss the critical BKT temperature as a function of the spin-orbit coupling strength λ , as shown in Fig. 7. Compared with the binding energy dependence and Zeeman field dependence, the dependence of T_{BKT} on the spin-orbit coupling strength is non-monotonic and the emerging superfluid phases can re-appear with increasing the coupling strength. Therefore, the T_{BKT} curve is more subtle to understand. Nevertheless, we may identify that the topologically trivial gFF superfluid phase tends to be favorable at large spin-orbit coupling. This is because the pairing gap is usually enhanced by the spin-orbit coupling, which makes the topological phase transition much more difficult to occur (cf. Eq. (27)). At small spin-orbit coupling, on the other hand, the critical BKT temperature may dramatically decrease to zero, particularly at a small binding energy and/or a large Zeeman field. Thus, for the purpose of observing the gapless topological tnFF phase, experimentally it seems better to use an intermediate spin-orbit coupling strength, i.e., $\lambda \sim E_F/k_F$.

IV. CONCLUSIONS

In summary, we have presented a systematic investigation of the Berezinskii-Kosterlitz-Thouless transition in a spin-orbit coupled atomic Fulde-Ferrell superfluid in two dimensions. We have calculated the superfluid density and superfluid transition temperature of various Fulde-Ferrell superfluids. We have paid special attention to an interesting gapless topological Fulde-Ferrell superfluid and have clarified that, by suitably tuning the external parameters - for example, the interatomic interaction strength, in-plane and out-of-plane Zeeman fields, and spin-orbit coupling strength - its observation is within the reach in current cold-atom experimental setups.

Our investigation is based on the mean-field theoretical framework, which is supposed to be applicable to a weakly interacting two-dimensional Fermi gas (i.e., the binding energy $E_b \leq 0.2E_F$). For a more reliable and quantitative description, in future studies it would be useful to take into account the strong phase fluctuations by using many-body T -matrix theories [63, 68, 69].

Acknowledgments

X.J.L. and H.H. were supported by the Australian Research Council (ARC) (Grants Nos. FT140100003, FT130100815, DP140103231 and DP140100637) and the National Key Basic Research Special Foundation of China (NKBRSCF-China) (Grant No. 2011CB921502). L.H. was supported by US Department of Energy Nuclear

Physics Office. G.L.L. was supported by the National Natural Science Foundation of China (NSFC-China) (Grant Nos. 11175094, 91221205) and the NKBRSCF-China (Grant No. 2011CB921602).

Note added. Recently, a similar publication by Xu and Zhang became public [70]. Results qualitatively agree where applicable.

-
- [1] P. Fulde and R. A. Ferrell, *Phys. Rev.* **135**, A550 (1964).
 [2] A. I. Larkin and Y. N. Ovchinnikov, *Zh. Eksp. Teor. Fiz.* **47**, 1136 (1964) [*Sov. Phys. JETP* **20**, 762 (1965)].
 [3] R. Casalbuoni and G. Nardulli, *Rev. Mod. Phys.* **76**, 263 (2004).
 [4] S. Uji, T. Terashima, M. Nishimura, Y. Takahide, T. Konoike, K. Enomoto, H. Cui, H. Kobayashi, A. Kobayashi, H. Tanaka, M. Tokumoto, E. S. Choi, T. Tokumoto, D. Graf, and J. S. Brooks, *Phys. Rev. Lett.* **97**, 157001 (2006).
 [5] M. Kenzelmann, Th. Str̄d̄ssle, C. Niedermayer, M. Sigrist, B. Padmanabhan, M. Zolliker, A. D. Bianchi, R. Movshovich, E. D. Bauer, J. L. Sarrao, and J. D. Thompson, *Science* **321**, 1652 (2008).
 [6] Y.-A. Liao, A. S. C. Rittner, T. Paprotta, W. Li, G. B. Partridge, R. G. Hulet, S. K. Baur, and E. J. Mueller, *Nature (London)* **467**, 567 (2010).
 [7] S. Gerber, M. Bartkowiak, J. L. Gavilano, E. Ressouche, N. Egetenmeyer, C. Niedermayer, A. D. Bianchi, R. Movshovich, E. D. Bauer, J. D. Thompson, and M. Kenzelmann, *Nature Phys.* **10**, 126 (2014).
 [8] G. Orso, *Phys. Rev. Lett.* **98**, 070402 (2007).
 [9] H. Hu, X.-J. Liu, and P. D. Drummond, *Phys. Rev. Lett.* **98**, 070403 (2007).
 [10] X.-J. Liu, H. Hu, and P. D. Drummond, *Phys. Rev. A* **76**, 043605 (2007).
 [11] X.-J. Liu, H. Hu, and P. D. Drummond, *Phys. Rev. A* **78**, 023601 (2008).
 [12] X.-W. Guan, M. T. Batchelor, C.-H. Lee, and M. Bortz, *Phys. Rev. B* **76**, 085120 (2007).
 [13] For the latest review, see, for example, S. K. Yip, *Annu. Rev. Condens. Matter Phys.* **5**, 15 (2014), and reference therein.
 [14] V. Barzykin and L. P. Gor'kov, *Phys. Rev. Lett.* **89**, 227002 (2002).
 [15] D. F. Agterberg and R. P. Kaur, *Phys. Rev. B* **75**, 064511 (2007).
 [16] O. Dimitrova and M. V. Feigel'man, *Phys. Rev. B* **76**, 014522 (2007).
 [17] K. Michaeli, A. C. Potter, and P. A. Lee, *Phys. Rev. Lett.* **108**, 117003 (2012).
 [18] Y.-J. Lin, K. Jim̄nez-García, and I. B. Spielman, *Nature (London)* **471**, 83 (2011).
 [19] P. Wang, Z.-Q. Yu, Z. Fu, J. Miao, L. Huang, S. Chai, H. Zhai, and J. Zhang, *Phys. Rev. Lett.* **109**, 095301 (2012).
 [20] L. W. Cheuk, A. T. Sommer, Z. Hadzibabic, T. Yefsah, W. S. Bakr, and M. W. Zwierlein, *Phys. Rev. Lett.* **109**, 095302 (2012).
 [21] Z. Fu, L. Huang, Z. Meng, P. Wang, X.-J. Liu, H. Pu, H. Hu, and J. Zhang, *Phys. Rev. A* **87**, 053619 (2013).
 [22] For a review, see for example, J. Zhang, X.-J. Liu, H. Hu, and H. Pu, *Fermi Gases with Synthetic Spin-Orbit Coupling*. In K. W. Madison, L. D. Carr, and H. Zhai (eds.) *Annual Review of Cold Atoms and Molecules* (volume 2): World Scientific Publishing, chap. 2 (2014).
 [23] L. Dong, L. Jiang, H. Hu, and H. Pu, *Phys. Rev. A* **87**, 043616 (2013).
 [24] Z. Zheng, M. Gong, X. Zou, C. Zhang, and G.-C. Guo, *Phys. Rev. A* **87**, 031602(R) (2013).
 [25] F. Wu, G.-C. Guo, W. Zhang, and W. Yi, *Phys. Rev. Lett.* **110**, 110401 (2013).
 [26] X.-J. Liu and H. Hu, *Phys. Rev. A* **87**, 051608(R) (2013).
 [27] L. Dong, L. Jiang, and H. Pu, *New J. Phys.* **15**, 075014 (2013).
 [28] X.-F. Zhou, G.-C. Guo, W. Zhang, and W. Yi, *Phys. Rev. A* **87**, 063606 (2013).
 [29] M. Iskin, *Phys. Rev. A* **88**, 013631 (2013).
 [30] V. B. Shenoy, *Phys. Rev. A* **88**, 033609 (2013).
 [31] C. Zhang, S. Tewari, R. M. Lutchyn, and S. Das Sarma, *Phys. Rev. Lett.* **101**, 160401 (2008).
 [32] M. Sato, Y. Takahashi, and S. Fujimoto, *Phys. Rev. Lett.* **103**, 020401 (2009).
 [33] J. D. Sau, R. M. Lutchyn, S. Tewari, and S. Das Sarma, *Phys. Rev. Lett.* **104**, 040502 (2010).
 [34] Y. Oreg, G. Refael, and F. von Oppen, *Phys. Rev. Lett.* **105**, 177002 (2010).
 [35] S.-L. Zhu, L. B. Shao, Z. D. Wang, and L. M. Duan, *Phys. Rev. Lett.* **106**, 100404 (2011).
 [36] X.-J. Liu, L. Jiang, H. Pu, and H. Hu, *Phys. Rev. A* **85**, 021603(R) (2012).
 [37] X.-J. Liu and H. Hu, *Phys. Rev. A* **85**, 033622 (2012).
 [38] R. Wei and E. J. Mueller, *Phys. Rev. A* **86**, 063604 (2012).
 [39] C. Chen, *Phys. Rev. Lett.* **111**, 235302 (2013).
 [40] X.-J. Liu and H. Hu, *Phys. Rev. A* **88**, 023622 (2013).
 [41] C. Qu, Z. Zheng, M. Gong, Y. Xu, L. Mao, X. Zou, G. Guo, and C. Zhang, *Nat. Comm.* **4**, 2710 (2013).
 [42] W. Zhang and W. Yi, *Nat. Comm.* **4**, 2711 (2013).
 [43] Y. Cao, S.-H. Zou, X.-J. Liu, S. Yi, G.-L. Long, and H. Hu, *Phys. Rev. Lett.* **113**, 115302 (2014).
 [44] H. Hu, L. Dong, Y. Cao, H. Pu, and X.-J. Liu, *Phys. Rev. A* **90**, 033624 (2014).
 [45] L. Jiang, E. Tiesinga, X.-J. Liu, H. Hu, and H. Pu, *arXiv:1404.6211* (2014).
 [46] V. L. Berezinskii, *Sov. Phys. JETP* **32**, 493 (1971).
 [47] J. M. Kosterlitz and D. Thouless, *J. Phys. C* **5**, L124 (1972); **6**, 1181 (1973).
 [48] M. Randeria, J.-M. Duan, and L.-Y. Shieh, *Phys. Rev. Lett.* **62**, 981 (1989); *Phys. Rev. B* **41**, 327 (1990).
 [49] V. P. Gusynin, V. M. Loktev, and S. G. Sharapov, *JETP* **88**, 685 (1999); **90**, 993 (2000).
 [50] V. M. Loktev, R. M. Quick, and S. G. Sharapov, *Phys.*

- Rep. **349**, 1 (2001).
- [51] L. He and X.-G. Huang, Phys. Rev. Lett. **108**, 145302 (2012).
- [52] M. Gong, G. Chen, S. Jia, and C. Zhang, Phys. Rev. Lett. **109**, 105302 (2012).
- [53] L. He and X.-G. Huang, Ann. Phys. (N.Y.) **337**, 163 (2013).
- [54] In our earlier work [43], we use the notation δ for in-plane Zeeman field and Ω_R for out-of-plane Zeeman field.
- [55] H. Hu, L. Jiang, X.-J. Liu, and H. Pu, Phys. Rev. Lett. **107**, 195304 (2011).
- [56] L. Jiang, X.-J. Liu, H. Hu, and H. Pu, Phys. Rev. A **84**, 063618 (2011).
- [57] K. Zhou and Z. Zhang, Phys. Rev. Lett. **108**, 025301 (2012).
- [58] E. Taylor, A. Griffin, N. Fukushima, and Y. Ohashi, Phys. Rev. A **74**, 063626 (2006).
- [59] N. Fukushima, Y. Ohashi, E. Taylor, and A. Griffin, Phys. Rev. A **75**, 033609 (2007).
- [60] D. R. Nelson and J. M. Kosterlitz, Phys. Rev. Lett. **39**, 1201 (1977).
- [61] L. Salasnich, P. A. Marchetti, and F. Toigo, Phys. Rev. A **88**, 053612 (2013).
- [62] S. Yin, J.-P. Martikainen, and P. Törmä, Phys. Rev. B **89**, 014507 (2014).
- [63] H. Hu, X.-J. Liu, and P. D. Drummond, Europhys. Lett. **74**, 574 (2006).
- [64] J. Tempere and S. N. Klimin, arXiv:1407.5474 (2014).
- [65] M. Z. Hasan and C. L. Kane, Rev. Mod. Phys. **82**, 3045 (2010).
- [66] X.-L. Qi and S.-C. Zhang, Rev. Mod. Phys. **83**, 1057 (2011).
- [67] M. G. Ries, A. N. Wenz, G. Zürn, L. Bayha, I. Boettcher, D. Kedar, P. A. Murthy, M. Neidig, T. Lompe, and S. Jochim, arXiv:1409.5373 (2014).
- [68] H. Hu, X.-J. Liu, and P. D. Drummond, Phys. Rev. A **77**, 061605 (2008).
- [69] H. Hu, X.-J. Liu, and P. D. Drummond, New J. Phys. **12**, 063038 (2010).
- [70] Y. Xu and C. Zhang, arXiv:1407.3483 (2014).